AGU PUBLICATIONS

Geochemistry, Geophysics, Geosystems

RESEARCH ARTICLE
10.1002/2015GC006047

Key Points:
- Cenozoic exhumation history of the Gangdese batholith from low temperature thermochronology
- Low exhumation rates commencing ~45 Ma suggest regional plateau formation by that time
- Miocene exhumation caused by incision of the paleo-Yarlung River

Supporting Information:
- Supporting Information S1
- Table S1
- Table S2

Correspondence to:
G. Li,
guangwei.li@unimelb.edu.au

Citation:
Li, G., B. Kohn, M. Sandiford, Z. Xu, Y. Tian, and C. Seiler (2016), Synorogenic morphotectonic evolution of the Gangdese batholith, South Tibet: Insights from low-temperature thermochronology, *Geochem. Geophys. Geosyst.*, *17*, 101–112, doi:10.1002/2015GC006047.

Received 13 AUG 2015
Accepted 5 DEC 2015
Accepted article online 14 DEC 2015
Published online 17 JAN 2016

Synorogenic morphotectonic evolution of the Gangdese batholith, South Tibet: Insights from low-temperature thermochronology

Guangwei Li[1], Barry Kohn[1], Mike Sandiford[1], Zhiqin Xu[2], Yuntao Tian[3], and Christian Seiler[1]

[1]School of Earth Sciences, University of Melbourne, Melbourne, Victoria, Australia, [2]State Laboratory for Continental tectonics and Dynamics, Institute of Geology, Chinese Academy of Geological Sciences, Beijing, China, [3]Department of Earth Sciences, University College London, London, UK

Abstract The uplift history of the Tibetan Plateau remains one of most intriguing and controversial issues in the Cenozoic history of our planet, and has a significant impact on regional and global climate. Here, we report new low-temperature thermochronology apatite and zircon data from the Gangdese batholith in southern Tibet. Thermal history modeling of the data show that the batholith experienced a phase of rapid Early Cenozoic cooling probably associated with exhumation resulting from the initial India-Asia's collision, but possibly also due to postarc volcanic activity in the region. The batholith, then transitioned to low erosion rates (<0.05 mm/yr) between the Middle Eocene and Early Miocene, followed by a renewed episode of cooling commencing in the Early Miocene. Our results indicate that the Gangdese belt, as the southern margin of Eocene Tibetan Plateau, became plateau-like by ~45 Ma. The later cooling episode from Early Miocene onward, can probably be attributed to incision of the ancestral Yarlung River system, cutting through the Gangdese belt by ~22 Ma at the latest.

1. Introduction

Uplift of the Tibet Plateau is a key Cenozoic geological event, which had a profound influence on both the regional and global climatic system [*Molnar et al.*, 2010]. Although the detailed uplift process (e.g., onset of uplift ranging from the Late Cretaceous to Late Miocene) and mechanism of Tibetan plateau growth (e.g., underthrusting or injection of the Indian plate, continuous deformation and crustal thickening, dynamic processes in the lower crust and mantle, intracontinental subduction of the Asian lithosphere) remains debatable [*Wang et al.*, 2014; *Li et al.*, 2015c, and references therein), in recent years many studies have emphasized that the rise of the Plateau was accompanied by an outward growth from central Tibet [e.g., *Tapponnier et al.*, 2001; *Kapp et al.*, 2007; *Wang et al.*, 2008, 2014; *Rohrmann et al.*, 2012; *Li et al.*, 2015c]. This proposition is also supported by the distribution of low-temperature thermochronology age data [e.g., *Rohrmann et al.*, 2012; *Li et al.*, 2015; references therein], which appears to young outward from an old central core (Figure 1). *Hetzel et al.* [2011] applied low temperature thermochronology and cosmogenic methods to what was described as a pre-Eocene near sea-level "low-relief" landscape in the northern Lhasa terrane. However, contrary to this view, it has been argued that slow exhumation in pre- and Eocene time led to the development of this low-relief landscape in a high elevation, internally drained setting [*Tian et al.*, 2013]. *Rohrmann et al.* [2012] used low-temperature thermochronology data from the interior Tibetan Plateau (see Figure 1) as evidence that a steady and slow erosion rate (<0.05 mm/yr) for the establishment of a central plateau (mainly including Lhasa and Qiangtang terranes) by ~45 Ma. Further, using paleoaltimetric evidence from carbon and oxygen isotopes, *Ding et al.* [2014] proposed that the Andean-type Gangdese arc at the southern margin of the Lhasa terrane had attained an elevation of ~4500 m since Late Cretaceous time. However, the question of when the Gangdese area became plateau-like still remains uncertain.

Data obtained using low-temperature thermochronology methods, such as apatite fission track (AFT) and zircon/apatite (U-Th)/He (ZHe/AHe), record the time elapsed since cooling of rock within temperature windows called the partial retention/annealing zone (ZHe: ~130–200°C; AFT ~60–120°C; AHe ~40–80°C), which is used to constrain the timing and rate of cooling and indirectly exhumation of rocks [*Gleadow et al.*, 2002; *Farley*, 2002; *Reiners et al.*, 2004]. To date, few available low-temperature thermochronology data constrain the early cooling and exhumation history of the Gangdese arc in the southern Lhasa terrane. Some data, however, have

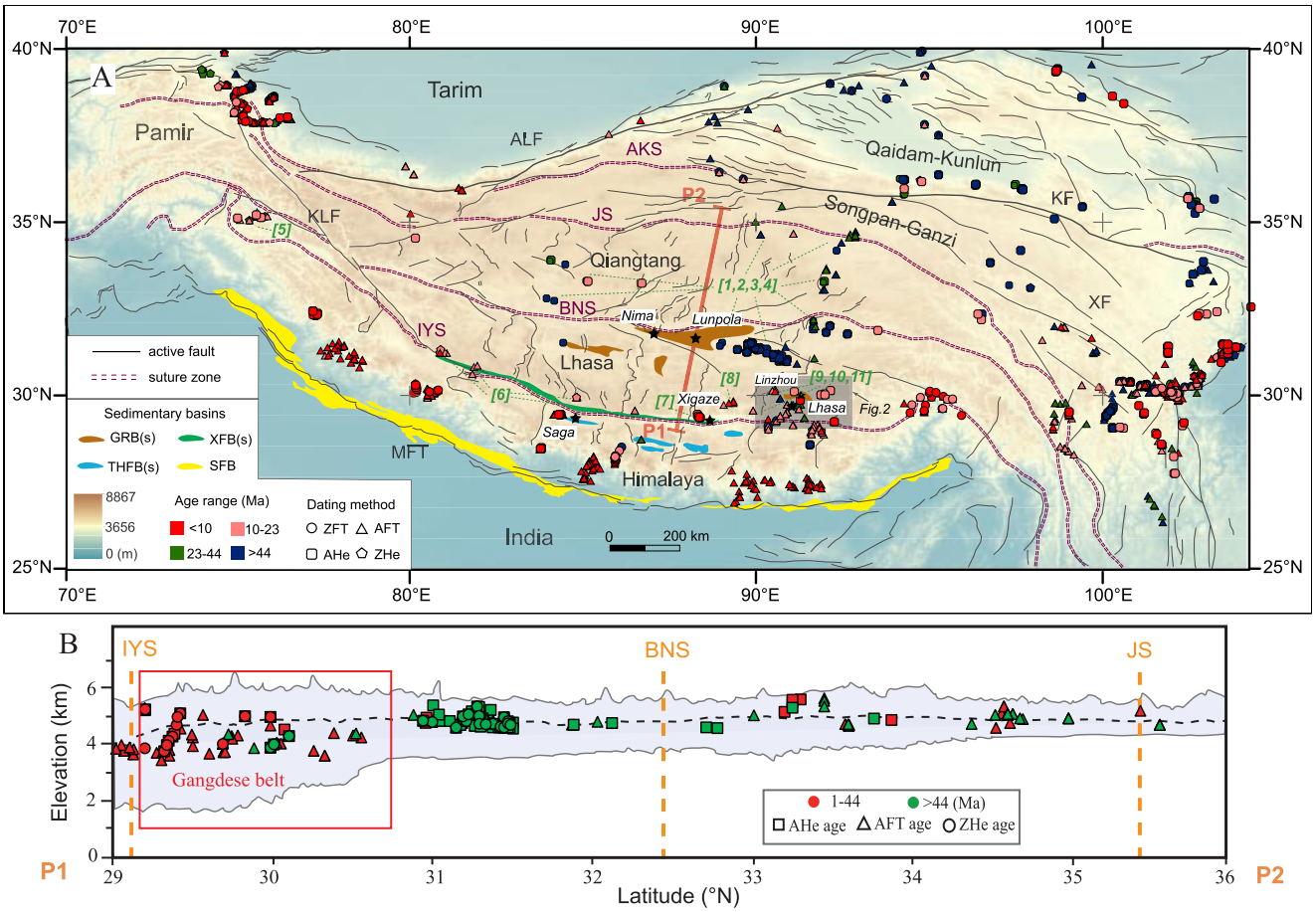

Figure 1. (a) DEM of the Tibetan Plateau with superimposed major structures, terranes, Cenozoic basins in South Tibet and thermochronologic data. References for Figure 1: (1) *Rohrmann et al.* [2012], (2) *Hetzel et al.* [2011], (3) *Haider et al.* [2013], (4) *Wang et al.* [2008], (5) *van der Beek et al.* [2009], (6) *Carrapa et al.* [2014], (7) *Dai et al.* [2013], (8) *Yuan et al.* [2007], (9) *Copeland et al.* [1987], (10) *Copeland et al.* [1995], (11) this study; other references are listed in the supporting information. IYS—Indus-Yarlung suture zone; BNS—Bangong suture; JS—Jinsha suture; AKS—Animaqing-Kunlun suture; ALF—Altyn Tagh Fault; KLF—Karakomrum Fault; KF—Karakash Fault; XF—Xianshuihe Fault; GRB—Cretaceous-Eocene Gangdese Retroarc Basin; XFB—Cretaceous Xigaze Forearc Basin; THFB—Late Cretaceous- Eocene Tethyan Himalyan Foreland basin; SFB—Oligocene-Miocene Siwalik Foreland Basin. (b) 800 km long topographic swath profile (P1–P2, see Figure 1) onto which low-T thermochronology ages from 85°E to 93°E are projected (ages from *Copeland et al.* [1995]; *Yuan et al.* [2007]; *Hetzel et al.* [2011]; *Rohrmann et al.* [2012]; *Dai et al.* [2013]; *Haider et al.* [2013]; *Li et al.* [2015b], and this study). This study concentrated on the Gangdese belt marked by a red rectangle.

been reported for the more recent history, e.g., a few Oligocene-Miocene AFT ages were reported from near Lhasa (without track length data) [*Copeland et al.*, 1987, 1995], Xigaze (without track length data) [*Yuan et al.*, 2007], Kailas [*Carrapa et al.*, 2014; *Wang et al.*, 2015], respectively. Further, *Dai et al.* [2013] suggested that ZHe and AHe ages from the middle part of Gangdese arc near Xigaze, may indicate a phase of Miocene cooling (Figure 1). It is worth noting that because these study areas are close to the Gangdese Thrust (GT) and Great Counter Thrust located at the southern margin of the Gangdese batholith, these cooling ages may have been linked to activity along these two major stuctures. In an effort to constrain the early stages of exhumation history of the Gangdese arc in the southern Lhasa terrane and further evaluate plateau formation in this region, this work reports a suite of ZHe, AFT and AHe data, as well as five zircon U-Pb ages.

2. Geological Setting and Sampling

The Lhasa terrane, located in central Tibet, is one of five main terranes forming the Tibetan Plateau (Figure 1). The extensive and widely exposed Late Triassic-Eocene Gangdese batholith, which intruded in the Paleozoic-Mesozoic units [*Chu et al.*, 2006; *Ji et al.*, 2009; *Zhu et al.*, 2011], forms a significant unit in the southern and central part of the terrane (Figure 2). The southern terrane mainly comprises the batholith units together with the Jurassic volcano-sedimentary sequence of the Yeba Formation (~190–174 Ma) [*Zhu et al.*, 2011] and Cenozoic volcanic rocks of the Linzizong Group (~64–40 Ma) [*Mo et al.*, 2008] (Figure 2).

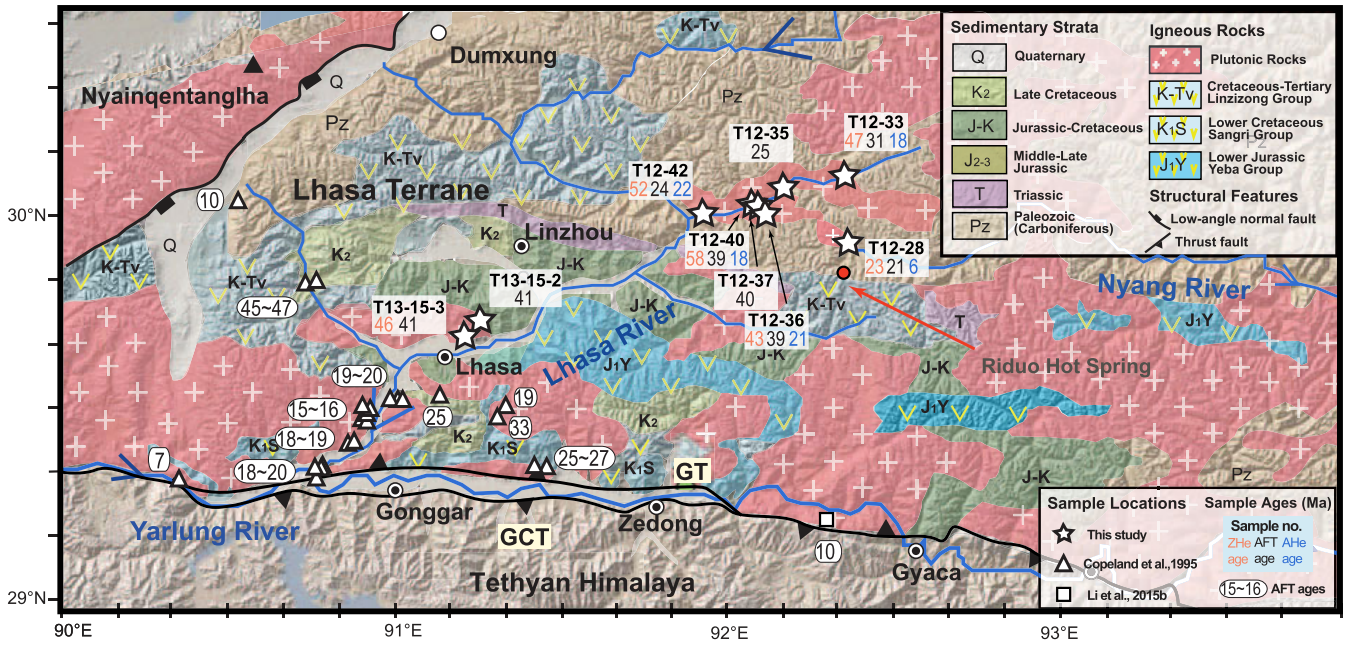

Figure 2. Simplified geologic map showing sample locations and the key drainage systems of the Gangdese belt in the southern Lhasa terrane (modified from *Kapp et al.* [2007]). GT—Gangdese Thrust; GCT—Great Counter Thrusts.

During the Late Miocene, an E-W extensional regime in the study area is indicated by development of the north-south trending Yangbajing-Yardong graben system [*Harrison et al.*, 1992] (Figures 1 and 2). In Oligocene-Early Miocene time, the north-dipping Gangdese Thrust (GT) and the Miocene, south-dipping Great Counter Thrust (GCT, locally named the Renbu-Zedong Thrust) systems developed along the southern margin of the Gangdese Batholith [*Quidelleur et al.*, 1997; *Yin*, 2006] (Figure 2).

The Cretaceous-Eocence basins in the Linzhou and Nima-Lunpola areas, considered as part of the Gangdese retroarc basin system, comprises lower Cretaceous marine limestone and upper Cretaceous-Eocene, dominantly fluvial sandstones and conglomerates [*Leier et al.*, 2007] (Figures 1 and 2). The Xigaze forearc basin deposited on the southern margin of the Lhasa terrane during Cretaceous – Early Cenozoic time, is mostly sourced from the Gangdese belt [*Wu et al.*, 2010]. To the south, the Indus-Yarlung suture zone (IYS) trends nearly east-west and separates sedimentary rocks of Indian affinity from the Lhasa terrane. The Late Oligocene-Miocene Gangrinboche conglomerates (including Gangrinboche, Qiuwu, Dazhuka), which are widely distributed along the IYS, were mainly derived from the Gangdese batholith [*DeCelles et al.*, 2011; *Wang et al.*, 2013] (Figure 2).

Samples were collected from the Gangdese Batholith in the southern Lhasa terrane, along two main northern tributaries of the Yarlung River, in the catchments of the Nyang (sample T12-28) and Lhasa Rivers (all other samples). Sample sites were located at elevation ranging from 3730 to 5003 m a.s.l., and are >50 km from active grabens (Figure 2 and Table 1; supporting information). Nine samples were collected from Mesozoic (7) and Early Cenozoic (2) Gangdese batholith granites. Three of them (T12-36, 37 and 40) were collected as an elevation profile over ~980 m across a late Triassic granite body (Figure 2). Most samples were located relatively far from the Linzizong volcanics, except for sample T12-28. Samples were analyzed using varying combinations of low-T thermochronology methods (AFT, ZHe and AHe systems) to characterize the cooling history of the terrane (Table 1 and supporting information). Furthermore, U/Pb zircon geochronology was also carried out on some of these samples to provide a more complete data set related to their emplacement ages (Table 1 and supporting information).

3. Analytical Methods

3.1. U-Pb Geochronology Analysis

Zircon crystals were concentrated using standard sample preparation techniques (crushing, heavy liquid and magnetic separation), and then mounted in epoxy resin. Cathodoluminescence (CL) images were used to check the internal structure of zircon grains and select potential target domains for in-situ U-Pb dating.

Table 1. U/Pb and Low-Temperature Thermochronology Age Data (This Study) From the Gangdese Belt

Sample Number	U-Pb Zircon Age[a,b] (Ma)	(U-Th)/He Zircon Age (Ma)[c,d]	Apatite Fission Track Age (Ma)[c,e]	(U-Th-Sm)/He Apatite Age[c,d] (Ma)
T12-28	197.8 ± 1.3	23.2 ± 1.6	21.3 ± 1.5	6.3 ± 0.5
T12-33		46.5 ± 3.3	31.0 ± 2.4	18.0 ± 1.3
T12-35	201.0 ± 2.1		24.8 ± 2.2	
T12-36	201.0 ± 1.6	43.3 ± 3.0	38.6 ± 2.4	21.2 ± 1.5
T12-37			40.2 ± 2.2	
T12-40	199.3 ± 2.5	58.0 ± 5.0	38.8 ± 2.5	18.1 ± 1.6
T12-42	198.9 ± 1.6	51.9 ± 3.8	23.5 ± 1.5	22.3 ± 2.0
T13-15-2	64.7 ± 1.1[f]		41.1 ± 2.9	
T13-15-3	64.7 ± 1.1[f]	45.8 ± 4.0	41.1 ± 3.4	

[a]Ages were obtained using laser ablation inductively coupled-plasma mass spectrometry dating of zircon.
[b]Reported error limits are ±2σ.
[c]Reported error limits are ±1σ.
[d]Weight mean age calculated by Isoplot 3.0.
[e]Pooled ages.
[f]Data from *Ji et al*. [2009].

U-Pb measurements were conducted at the School of Earth Sciences, University of Melbourne, employing a 193 nm ArF Excimer laser connected to an Agilent 7500a quadruple inductively coupled-plasma- mass-spectrometer (ICP-MS). Analytical methods followed those described by *Woodhead et al*. [2004, 2007], and *Paton et al*. [2010]. The Plesovice, TEMORA and 91500 zircon standards were analyzed along with zircon crystals of unknown U-Pb age from the Gangdese batholith to correct for U-Pb fractionation. Data reduction and correction for fractionation effects were conducted offline using Iolite [*Paton et al*., 2010], which runs on the Igor Pro software of Wavemetrics [*Hellstrom*, 2008]. Crystallization ages reported here (Table 1; see also supporting information) were calculated as the weighted mean of individual, concordant spot analyses using the $^{206}Pb/^{238}U$ ages, since the $^{207}Pb/^{235}U$ and $^{207}Pb/^{206}Pb$ ages are less precise for young granites.

3.2. Apatite Fission Track (AFT) Thermochronology

Apatite grains were concentrated using standard heavy liquid and magnetic separation procedures before being mounted in epoxy resin on glass slides, ground and polished to an optical finish to expose internal grain surfaces. Polished mounts were etched in 5M HNO_3 for 20 s at 20°C to reveal fossil tracks. A gold coating (∼5–7 nm thickness) was applied to the etched mounts to reduce reflections from grain boundaries under the microscope [*Gleadow et al*., 2009]. Apatite grains with polished surfaces parallel to prismatic crystal faces and homogeneous track distributions were selected using a Zeiss Axio Imager M1m microscope. A series of high-resolution digital images were then captured in both reflected and transmitted light at a total magnification of x1000 using a 3.2MP camera (pixel calibration of ∼0.0698–0.0705 μm/pixel). Automated counting of fission tracks was performed using the coincidence mapping protocol [*Gleadow et al*., 2009]. Uranium measurements of selected grains were carried out using LA-ICP-MS analysis [*Hasebe et al*., 2004]. In this case a NewWave UP213 Nd: YAG laser (single spot analysis using a 30 μm spot size, ∼2.0 J/cm2 energy and 5 Hz repetition rate), connected to an Agilent 7700x quadrupole ICP-MS. Trace element signals were normalized against ^{43}Ca using NIST-612 as a reference standard. The overall performance of the system was monitored against an internal apatite standard (Mud Tank: ∼3ppm ^{238}U).

Confined track length measurements were made on *c*-axis parallel grains as true 3D lengths using captured digital images. Where possible, more than 100 confined lengths were measured per sample. ^{252}Cf tracks were implanted into polished grains to increase the number of confined track-in-tracks (TINTs) suitable for length measurements, thus providing a more robust data set for inverse thermal history modeling. Etch pit diameters (Dpar) of all analyzed grains (age/length), were determined and used as kinetic parameters during thermal history modeling.

3.3. Apatite and Zircon U-Th/He Analysis

For U-Th/He analysis, inclusion-free apatite and zircon grains were hand-picked from concentrated separates after examination under polarized light. Ages were corrected for alpha ejection (FT correction) [*Farley et al*., 1996]. He extraction was performed using established laboratory routines [e.g., *House et al*., 2002]. Apatite and zircon aliquots were loaded into platinum capsules and outgassed under vacuum at ∼900°C for 5 min and ∼1300°C for 15 min, respectively, using a fiber-optically coupled diode laser with a 820 nm wavelength. ^{4}He abundances were determined as an isotope ratio using a pure ^{3}He spike that has been calibrated against an independent ^{4}He standard. The uncertainty in the sample ^{4}He measurement is estimated

at <1%. Apatite U-Th-Sm data were obtained using an Agilent 7700 quadrupole ICP-MS after total dissolution of the outgassed apatite aliquots in HNO_3. For zircon U-Th data, aliquots were transferred to Parr bombs where they were spiked with ^{235}U and ^{230}Th and digested at 240°C for 40 h in HF. Standard solutions containing the same spike amounts as samples were treated identically, as were a series of unspiked reagent blanks. A second bombing in HCl for 24 h at 200°C ensured dissolution of fluoride salts and final solutions were diluted to 10% acidity for analysis on an Agilent 7700 quadrupole ICP-MS. Analytical uncertainties for the University of Melbourne U-Th/He facility are estimated at ~6.2% (± 1σ), which incorporates an α-correction related constituent and takes into account an estimated 5 μm uncertainty in grain size measurements, gas analysis and ICP-MS uncertainties. Durango apatite and Fish Canyon Tuff zircon were run as internal standards with each batch of samples and served as an additional check internal monitor for analytical accuracy. Furthermore, weighted mean ages of AHe and ZHe are used for discussing individual sample cooling age and the number of single grains analyzed per sample is shown in the supporting information.

4. Results

4.1. U-Pb Zircon Ages for Granitoids

Five granitoid samples ~90 km northeast of Lhasa yield U-Pb zircon ages ranging between 201.0 ± 1.6 and 197.8 ± 1.3 Ma (Table 1; see supporting information). These ages are similar to $^{40}Ar/^{39}Ar$ biotite and hornblende cooling ages of ~ 200 Ma reported by *He et al*. [2006], suggesting that granite emplacement occurred at relatively shallow crustal levels resulting in rapid conductive cooling.

4.2. AFT Data

Nine AFT pooled ages range from ~ 21 ± 1.5 to 41 ± 2.9 Ma. Their non-projected track mean lengths are relatively short, ranging between 10.5 ± 3.7 and 12.5 ± 2.4 μm (Table 2), and mean Dpar values vary from 1.36 to 2.42 μm (Table 2). Three samples from the elevation profile (T12-36, -37 and -40) yield concordant AFT ages of ~ 40 Ma (Tables 1 and 2).

4.3. AHe and ZHe Data

Three samples collected along the floor of the Lhasa River valley (T12-33, −40 and −42), yield slightly older weighted mean AHe ages southward trending from ~18 ± 1.3 to 22.3 ± 2.0 Ma (Figure 2 and supporting information Figure S2). A sample collected from the elevation profile on a ridge bordering the Lhasa valley (T12-36) yielded a slightly older AHe age of ~ 21.2 ± 1.5 Ma, than one (T12-40) from the valley floor a ~18 ± 1.6 Ma. All of these are significantly older than sample T12-28 from the Nyang River valley, which yields a Late Miocene weighted mean age of ~6.4 ± 0.5 Ma (Table 1 and supporting information).

Six ZHe ages range from ~58.0 ± 5.0 to ~23.2 ± 1.6 Ma with the majority (5 of 6) yielding Paleocene-Eocene ages, except for sample T12-28 with an Early Miocene age of ~23.2 ± 1.6 (Tables 1 and supporting information). In addition, there is no correlation between Helium ages and its eU content of each sample (supporting information Figure S3) .

5. Thermal Modeling and Interpretations

To better constrain the thermal history of samples, the results from AFT, ZHe and AHe analyses were modeled in combination where possible using the inverse approach of HeFTy program [*Ketcham*, 2005], which uses a Kolmogorov-Smirnov (K-S) test to compare the predictions of a thermal history model to observations [*Ketcham*, 2005], thus ruling out the use of inappropriate models [*Vermeesch and Tian*, 2014].

5.1. Thermal History Modeling Strategy

AFT data were modeled using the multikinetic annealing model of *Ketcham et al*. [2007], using Dpar as a kinetic parameter; AHe data were modeled using the radiation damage accumulation and annealing model (RDAAM) [*Flowers et al*., 2009]; and ZHe data were modeled using the helium diffusion model of *Guenthner et al*. [2013]. Constraints used for the thermal history modeling were as follow: (i) Present-day mean surface temperature of 10 ± 5°C; (ii) Where applicable, broad temperature constraints 150–200°C were set around the time range covering the ZHe ages with 2σ to set an initial box; (iii) C-axis projected track length data

Geochemistry, Geophysics, Geosystems

10.1002/2015GC006047

Table 2. Apatite Fission Track Data From the Gangdese Batholith Near Lhasa

	Sample Information				Age Results							Track Length Results[a]			
					Spontaneous Tracks							Measured	*c*-Axis[e] Projected		
Sample No.	Lithology	Locality (°E/°N)	Elevation (m)	No. of Grains (n)	No. (n)	Density (10^5 cm^{-2})	Mean[b] ^{238}U and SD (ppm)	Pooled Age[c] (Ma±1 σ)	P(χ^2) (%)	Dispersion (%)	Central Age[d] (Ma±1 σ)	Mean (μm ± 1 SD)	Mean (μm ± 1SD)	No. (n)	Mean Dpar (Range) (μm)
T12-28	diorite	91.320/29.822	5003	24	166	1.637	14.5 ± 3.9	21.3 ± 1.5	65	18	22.5 ± 1.8	10.5 ± 3.7	12.8 ± 1.9	159	1.76 (1.6–2.0)
T12-33	granite	92.188/30.098	4302	30	191	1.877	11.3 ±5 .7	31.0 ± 2.4	58	7	33.5 ± 2.5	11.2 ± 2.1	12.7 ± 1.4	154	1.42 (1.3–1.8)
T12-35	granite	92.052/30.022	4062	34	237	1.930	15.1 ± 9.8	24.8 ± 2.2	75	20	26.3 ± 2.0	12.5 ± 2.4	13.8 ± 1.5	128	1.73 (1.4–1.9)
T12-36	granite	92.025/29.981	4982	32	535	3.117	15.3 ± 2.8	38.6 ± 2.4	64	18	39.7 ± 2.2				
T12-37	granite	92.022/29.983	4670	26	374	4.058	19.2 ± 5.3	40.2 ± 2.2	56	2	41.4 ± 2.2	12.4 ± 1.7	13.6 ± 1.2	159	1.97 (1.7–2.1)
T12-40	granite	92.010/30.003	4003	35	384	3.083	15.4 ± 5.3	38.8 ± 2.5	76	19	39.7 ± 2.5				
T12-42	granite	91.910/29.981	3890	34	345	1.935	15.5 ± 3.8	23.5 ± 1.5	58	6	24.6 ± 1.4	10.8 ± 3.1	12.8 ± 1.7	119	1.36 (1.2–1.5)
T13-15-2	granite	91.336/29.698	3730	23	140	1.492	6.6 ± 1.5	41.1 ± 2.9	57	8	45.8 ± 3.9	10.7 ± 3.3	12.9 ± 1.7	165	1.95 (1.7–2.2)
T13-15-3	granite	91.267/29.683	4013	21	101	1.127	4.8 ± 2.8	41.1 ± 3.4	40	10	46.0 ± 4.8	11.9 ± 2.7	13.4 ± 1.6	148	2.42 (1.9–3.0)

[a]Lengths measured after ^{252}Cf irradiation.
[b]Mean uranium content of all grains measured by LA-ICP-MS; SD, standard deviation.
[c]Pooled AFT ages of all grain.
[d]Central age calculated using RadialPlotter [*Vermeesch*, 2009].
[e]*C*-axis projected mean track lengths after [*Ketcham et al.*, 2007].

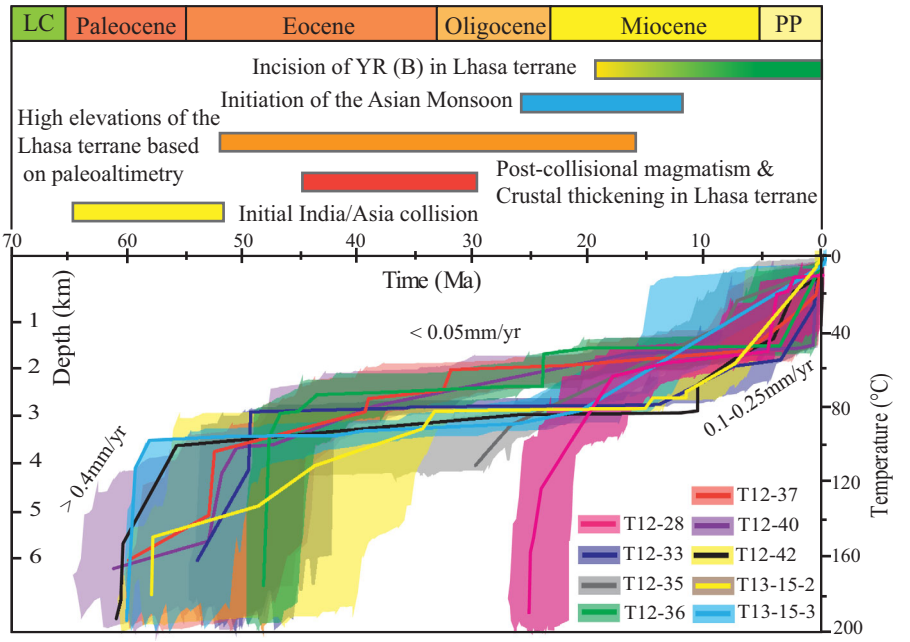

Figure 3. Cooling history of the Mesozoic-Cenozoic Gangdese batholith and geologic events in southern Tibet. (a) Timing of important geologic events in southern Tibet, shown by horizontal bars below geologic time scale. Geologic events compiled from *Rohrmann et al.* [2012] (YR (B) incision); *Sun and Wang* [2005] (onset of Asian Monsoon); *Spicer et al.* [2003], *Rowley and Currie* [2006], and *Ding et al.* [2014] (paleoaltimetry); *Chung et al.* [2009] (crustal thickening of the Lhasa terrane); *Ding et al.* [2005] (India/Asia collision). (b) Cooling histories of nine samples based on thermal history modeling of ZHe, AHe and AFT data. Envelopes encompass all of "Good Fit" models obtained for the nine samples using a merit value of 0.5 in HeFTy, while thick lines represent best-fit models to analytical data [*Ketcham*, 2005]. Details of modeling results are shown in supporting information. LC—Late Cretaceous; P-P—Pliocene to present; YR (B)—Yarlung River (its tributaries).

were applied. These premodeling settings were always included with large uncertainties so as to give the inversion algorithm sufficient freedom to search for a wide range of possible thermal histories.

Five samples (T12-28, 33, 36, 40 and 42) were modeled using combined ZHe, AHe and AFT data; one samples (T13-15-3) used ZHe and AFT data and only AFT data were used for sample (T12-35) (Table 1 and Figure 3; supporting information). The other two samples were modeled using constraints based on neighbouring samples (e.g., T12-37 was modeled using the ZHe and AHe ages of nearby samples T12-36 and T12-40, which have the same AFT age, while samples T12-36 and T12-40 were modeled using length data of T12-37; T13-15-2 was modeled using ZHe ages of nearby sample T13-15-3, which yield the same zircon U-Pb age). Inverse thermal history modeling was run until 100 good paths were obtained, which in most cases resulted in >1000 acceptable paths.

5.2. Thermal History Modeling Results

Thermal models history reveal a cooling record from ~200°C to <40°C between ~60 Ma and the present-day (Figure 3 and supporting information). The models show that seven of the nine samples experienced rapid Paleocene to Early Eocene cooling (>10°C/Ma), before cooling rates slowed dramatically to <~1.5°C/Ma between the Eocene (~ 45 Ma) and Early Miocene, followed by increased cooling (3–6°C/Ma) from the Miocene (Figure 3 and supporting information). The other two samples T12-35 (AFT: 24.8 ± 2.2 Ma) and T12-28 (ZHe: 23.2 ± 1.6 Ma; AFT: 21.3 ± 1.5 Ma; AHe: 6.3 ± 0.5 Ma) yield the youngest ages and only record the younger cooling episode (Figure 3 and supporting information). Assuming denudation-induced cooling and a paleogeothermal gradient of 25–30°C/km, the above cooling rates suggest that exhumation rates slowed down to about 0.05–0.02 mm/yr during the Eocene-Early Miocene following an earlier phase of relatively rapid Late Cretaceous-Eocene exhumation (>0.4 mm/yr). Exhumation in the Miocene accelerated slightly to moderate rates of 0.25–0.1mm/yr (Figure 3), broadly consistent with results reported from the northern Lhasa and Qiangtang terrenes [*Hetzel et al.*, 2011; *Rohrmann et al.*, 2012; *Haider et al.*, 2013] and northwest Himalaya [*van der Beek et al.*, 2009].

6. Discussion

6.1. Evolution of the Gangdese Batholith

6.1.1. Late Cretaceous-Middle Eocene

It has been well documented that the Gangdese batholith probably formed an elevated Andean-type mountain range stretching along the southern margin of the Lhasa terrane prior to India-Asia collision [e.g., *England and Searle*, 1986; *Kapp et al*., 2007; *Ding et al*., 2014]. The existence of elevated topography is supported by several studies of Late Cretaceous-Paleogene basins in the Lhasa terrane and adjacent areas to the south, which proposed that the elevated paleo-Gangdese landscape acted as a key sediment source region for nearby basins [*Tian et al*., 2013, references therein]. For example, in the Lhasa terrrane, the Late Cretaceous fluvial Takena Formation and Paleocene-Eocene Nianbo and Pana Formations near Linzhou and the Cretaceous Selinco basin near Nima-Lunpola, were deposited in a retroarc terrestrial foreland basin setting (Figure 1), and all are inferred to have been sourced from the Gangdese belt [*Kapp et al*., 2007; *Ding et al*., 2009, 2014]. To the south, Xigaze forearc basin sequences [*Wu et al*., 2010] and the foreland basins in south Tibet [*Ding et al*., 2005; *DeCelles et al*., 2014], were mainly derived from the proximal Gangdese batholith.

Data from the Gangdese batholith reported herein suggest that this belt experienced a rapid cooling episode prior to the Middle Eocene, which coincides with the cessation of the main activity of Gangdese magmatism and volcanism at around ~40 Ma [e.g., *Zhou et al*. 2004; *Zhu et al*., 2011, references therein] (Figure 2). Thus, this cooling episode is possibly related to the postmagmatic relaxation of the geothermal gradient. However, our samples were located away from areas of Linzizong volcanics (see Figure 2), therefore the cooling recorded by our samples is more likely related to regional rapid exhumation resulting from the onset of India-Asia collision. Collectively, at this stage the Gangdese belt, probably formed a typical Andean-type mountain chain located at the southern margin of the Lhasa terrane, as a long-lived Cenozoic drainage divide along southern margin of the Lhasa terrane, acting as a sedimentary source for foreland basins (Linzhou Basin and Lunpola-Nima basin) formed by the Gangdese retroarc thrust and Bangong suture zone [*Kapp et al*., 2007; *Ding et al*., 2009] to the north and Xigaze forearc basin and foreland basins along the Indus-Yarlung suture zone to the south [*Ding et al*., 2005; *Wu et al*., 2010; *DeCelles et al*., 2014] (Figure 4a).

6.1.2. Middle Eocene-Early Miocene (~45–23 Ma)

As mentioned previously, it has been proposed that central Tibet (Lhasa and Qiangtang terranes, Figure 1a) had attained a high elevation by the early Eocene and throughout the Neogene expanded toward the present southern and northern margins of the Tibetan Plateau [*Wang et al*., 2008, 2014; *Rohrmann et al*., 2012; *Li et al*., 2015]. The onset of low erosion rates (e.g., $<$0.05 mm/yr) is used as an indicator for the establishment of a plateau in Tibet (*van der Beek et al*., 2009; *Rohrmann et al*., 2012]. Our results show that, by ~ 45 Ma, exhumation rates of the Gangdese arc had slowed significantly, and that a subdued erosional regime continued until the early Miocene (Figure 3). This observation is comparable with those from the northern Lhasa and Qiangtang terranes [*Hetzel et al*., 2011; *Rohrmann et al*., 2012; *Haider et al*., 2013] and northwestern Himalaya [*van der Beek et al*., 2009]. Furthermore, paleoaltimetry studies (e.g., carbon and oxygen stable isotopes) of the Lhasa terrane suggest that central Tibetan Plateau was uplifted to near-modern elevations by the Eocene-Oligocene [*Rowley and Currie*, 2006; *Quade et al*., 2011; *Ding et al*., 2014]. This finding is consistent with the magmatic evolution of the Lhasa terrane indicating that the crust thickened substantially during the Eocene-Oligocene [*Chung et al*. 2009]. We agree with the interpretation of *Rohrmann et al*. [2012] that the low erosion rates of central Tibet ($<$0.05 mm/yr) represent the establishment of a regional relatively low-relief landscape at high elevation. Furthermore, our findings extend the regional low-relief surface southward to the Lhasa city area, and suggest that most of the Gangdese batholith had attained a plateau-like landscape by around ~45 Ma.

By contrast, the southernmost Gangdese batholith has relatively younger low-T thermochronology (ZHe, AHe and AFT) ages, most of them less than 30 Ma [*Copeland et al*., 1987, 1995; *Dai et al*., 2013; *Carrapa et al*., 2014; *Li et al*., 2015b] (Figures 1 and 2), which indicating that it underwent substantially greater exhumation and does not record cooling prior to the Oligocene. This is probably related to initiation of slip of the Gangdese Thrust at ~30 Ma and activity of the GCT between ~19–10 Ma, along the southern boundary of the Gangdese batholith [*Yin*, 2006] (Figure 2) or the combined effect of postcollisional deformation (both contractional and extensional) coupled with incision of the paleo-Yarlung starting at ~22 Ma [e.g., *DeCelles et al*., 2011; *Carrapa et al*., 2014; *Wang et al*., 2015]. During that time the Lhasa terrane likely formed to be

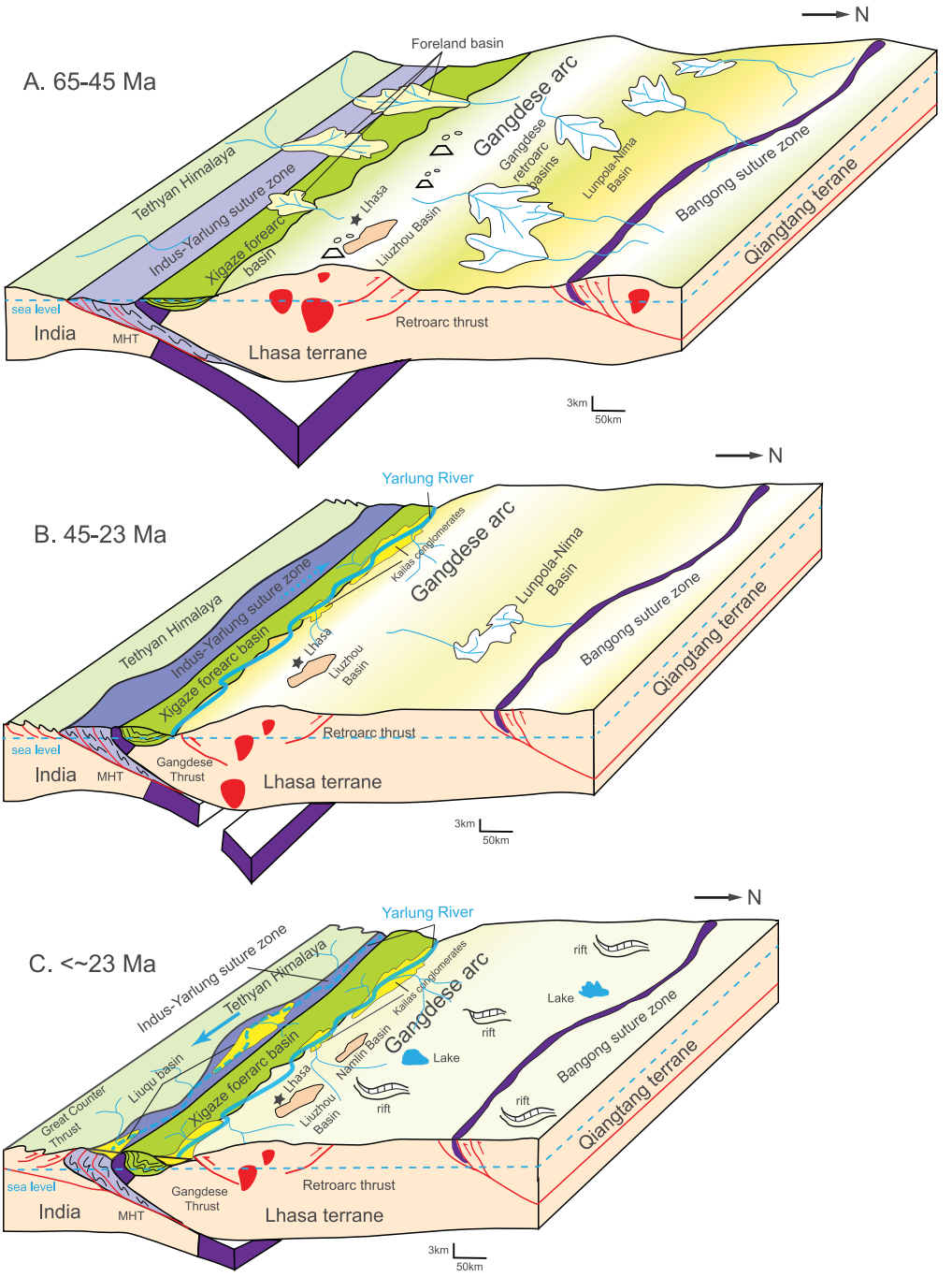

Figure 4. Late Cretaceous to Miocene tectonic model of Gangdese batholith based on new and published data (modified from *Ding et al.* [2014]). (a) ~65–45 Ma, the Gangdese batholith, formed a typical Andean-type mountain belt with a drainage divide along the southern margin of the Lhasa terrane, providing source material for the Gangdese retroarc basins to the north and foreland basins the south. (b) ~45–23 Ma, central Tibet formed a plateau (including Gangdese area), the Gangdese batholith also acted as a main source for fluvial basins to the north and south. (c) < ~23Ma, the Yarlung River commenced incision into the interior plateau, cutting through the Gangdese batholith. Ongoing indentation of the India plate continued northward, an E-W rift system developed in southern Tibet and extended to the north (currently active, see relevant references in the text). MHT—Main Himalayan Thrust (currently active).

plateau-like, while the southernmost Gangdese batholith located on the south margin of the Lhasa terrane resembled the present Himalayan ridge. As such it could have acted as a drainage divide, supplying most of the sediment to the Oligocene section of the lower part of the Gangrinboche/Kailas basin to the south [*DeCelles et al.*, 2011; *Wang et al.*, 2013], as well as the interior fluvial Namlin basin and Lunpola-Nima basin to the north [*Ding et al.*, 2009] (Figure 4b).

6.1.3. Early Miocene to present (<~23 Ma)

Previously published Miocene AFT and AHe data [*Copeland et al*., 1987, 1995; *Yuan et al*., 2007; *Rohrmann et al*., 2012; *Dai et al*., 2013; *Haider et al*., 2013] combined with the new data and models reported here (Table 1), indicate a relatively rapid cooling episode commencing in the Miocene (Figure 3, and supporting information Figure S5). This cooling is most likely associated with increased incision of the Lhasa River [*Rohrmann et al*., 2012], which may be a response to the establishment of external drainage by a connection between the Yarlung and Siang-Brahmaputra rivers in the Early Miocene [e.g., *Najman et al*., 2012; *Lang and Huntington*, 2014], as well as the possible intensification of the Asian monsoon [*Sun and Wang*, 2005]. The northward younging of AHe ages from samples along the Lhasa River valley (Figure 2 and Table 1; supporting information), suggests that the river commenced incision of the plateau to the northeast of Lhasa prior to ~22 Ma and has continued headward erosion northward to the present. The upper part of Kailas/Gangrinboche conglomerates (ca. 22–21 Ma) [*DeCelles et al*., 2011; *Carrapa et al*., 2014], widely distributed along the IYSZ, were mainly derived from the Gangdese batholith [*DeCelles et al*., 2011], confirming significant erosion of the batholith during that period [*Carrapa et al*., 2014].

Compared to other samples, T12-28 appears to have experienced much faster Early Miocene cooling from >200°C to yield young ZHe (~23Ma) and AFT (~22Ma) ages. This sample is located at the head of the Nyang River near the Riduo Hot Springs and Linzizong volcanic rocks (Figure 2), and was quite possibly affected by localized hydro-thermal heating during the early Miocene, a known overprinting mechanism for low-T thermochronometers [e.g., *Seiler et al*., 2009]. The young AHe age (~6.4 Ma) for this sample may have resulted either from enhanced incision of the Nyang River or may have been thermally reset by further local hydrothermal perturbations.

Generally, the observed Miocene cooling episode of the Gangdese batholith, mainly reflects incision toward the Tibetan Plateau interior (Figure 4c). It is worth noting that the Late Miocene cooling episode also prevailed in the other areas in southern Tibet (e.g., Nyainqentanglha area in Figure 2), where it has been related to rifting as part of an E-W extensional system [*Harrison et al*., 1992; *Yin*, 2006] (Figures 1 and 2)

6.2. Incision of the Yarlung River in South Tibet

As mentioned above, the relatively rapid Miocene cooling in the Gangdese batholith is probably related to incision of the Yarlung River and its tributaries. This corresponds well with proposed incision reported from thermochronological studies in neighboring areas along the Indus-Yarlung suture zone. For instance, rivers near Lhasa have been incising into the interior plateau since no later than ~15 Ma [*Rohrmann et al*., 2012]. *Dai et al*. [2013] also proposed enhanced Middle Miocene incision of the Yarlung River in the Xigaze area. *Carrapa et al*. [2014] suggested significant volume of rocks from the India-Asia collision zone (Indus-Yarlung suture zone - Figure 1) were removed in the Early Miocene based on thermochronological data of the Kailas Formtaiton and Gangdese batholith; this was interpreted to be the result of vigorous incision by the Yarlung River in the Miocene. *Li et al*. [2015b] suggested that pronounced Middle Miocene cooling in the Zedang area (Figure 2) was also probably caused by incision of branches of the Yarlung River. The study on the Liuqu conglomerate within the Indus-Yarlung suture zone, indicates that post Early Miocene exhumation of the Indus-Yarlung suture zone continued until ~6–8 Ma, which also probably resulted from incision of the Yarlung River [*Li et al*., 2015a]. This pattern of cooling/exhumation related to incision of the Yarlung River is consistent with the onset of the connection between the Yarlung and Siang-Brahmaputra (to the southeast) rivers in the Early Miocene [*Najman et al*., 2012; *Lang and Huntington*, 2014]. The establishment of an external drainage system by the Yarlung river since the Early Miocene, probably enhanced its regional ability of erosion, as well as facilitating headward incision of its tributaries into the Lhasa terrane (the interior of the plateau) to the north and the Tethyan Himalaya to the south.

7. Conclusions

New thermochronology data from the Gangdese belt in the Lhasa terrane combined with previous data confirm that central Tibet experienced an episode of rapid cooling/denudation during Latest Cretaceous to Early Eocene time. This cooling was associated with regional exhumation, coincident with onset of the India and Asia collision, as well as possibly reflecting postmagmatic relaxation of the geothermal gradient. During Eocene-Oligocene time, the region then experienced a period of relative erosional stability with slow denudation rates (0.05–0.02 mm/yr), followed by renewed more rapid cooling/denudation commencing in the

Miocene. These findings support the idea that the central Tibetan Plateau had formed by ~ 45 Ma. Thermal history modeling results and Early Miocene AHe ages from samples along the Lhasa River valley indicate that the Indus-Yarlung drainage system had already incised through parts of the central Plateau by ~22 Ma. However, Miocene exhumation of the southernmost Gangdese batholith was probably mainly controlled by activity along major structures, especially the GT and GCT. Furthermore, during the Late Cretaceous to Miocene, the Gangdese batholith probably acted as a drainage divide along the southern margin of the Lhasa terrane, providing a sediment source for contemporary basins to its north and south.

Acknowledgments

Funding for this research was provided by an Australian Research Council DECRA (Discovery Early Career Research Award, DE120102245) and China National Nature Science Foundation (41430212). The University of Melbourne thermochronology laboratory receives infrastructure support under the National Collaborative Research Infrastructure Strategy AuScope program. We thank anonymous reviewers and Paul Kapp and Peter van Beek for their helpful suggestions for improving the manuscript and Cin-Ty Lee for editorial handling. We are grateful to Abaz Alimanovic for assistance with (U-Th)/He dating and Hanwen Dong and Jianan Zhao for help with field work.

References

Carrapa, B., D. Orme, P. DeCelles, P. Kapp, M. Cosca, and R. Waldrip (2014), Miocene burial and exhumation of the India-Asia collision zone in southern Tibet: Response to slab dynamics and erosion, *Geology*, *42*(5), 443–446, doi:10.1130/G35350.1.

Chu, M. F., S. L. Chung, B. Song, D. Liu, S. Y. O'Reilly, and N. J. Pearson (2006), Zircon U-Pb and Hf isotope constraints on the Mesozoic tectonics and crustal evolution of southern Tibet, *Geology*, *34*, 745–748.

Chung, S., M. F. Chu, J.-Q. Ji, S. Y. O'Reilly, N. J. Pearson, D. Y. Liu, T. Y. Lee, and C. H. Lo (2009), The nature and timing of crustal thickening in southern Tibet: Geochemical and zircon Hf isotopic constraints from postcollisional adakites, *Tectonophysics*, *477*, 36–48.

Copeland, P., T. M. Harrison, W. S. F. Kidd, R. H. Xu, and Y. Q. Zhang (1987), Rapid early Miocene acceleration of uplift in the Gangdese Belt, Xizang-southern Tibet, and its bearing on accommodation mechanisms of the India-Asia collision, *Earth Planet. Sci. Lett.*, *86*, 240–252.

Copeland, P., T. M. Harrison, Y. Pan, W. S. F. Kidd, M. Roden, and Y. Q. Zhang (1995), Thermal evolution of the Gangdese Batholith, southern Tibet: A history of episodic unroofing, *Tectonics*, *14*, 223–236.

Dai, J., C. Wang, J. Hourigan, Z. Li, and G. Zhuang (2013), Exhumation history of the Gangdese Batholith, Southern Tibetan Plateau: Evidence from Apatite and Zircon (U-Th)/He thermochronology, *J. Geol.*, *121*(2), 155–172.

DeCelles, P., P. Kapp, J. Quade, and G. E. Gehrels (2011), Oligocene–Miocene Kailas basin, southwestern Tibet: Record of postcollisional upper plate extension in the Indus-Yarlung suture zone, *Geol. Soc. Am. Bull.*, *123*, 1337–1362, doi:10.1130/B30258.1.

DeCelles, P., P. Kapp, G. Gehrels, and L. Ding (2014), Paleocene-Eocene foreland basin evolution in the Himalaya of southern Tibet and Nepal: Implications for the age of initial India-Asia collision, *Tectonics*, *33*, 824–849, doi:10.1002/2014TC003522.

Ding, L., P. Kapp, and X. Wan (2005), Paleocene-Eocene record of ophilite obduction and initial India–Asian collision, south central Tibet, *Tectonics 24*, TC3001, doi:10.1029/2004TC001729.

Ding, L., F. Cai, Q. Zhang, L. Zhang, Q. Xu, D. Yang, D. Liu, and D. Zhong (2009), Provenance and tectonic evolution of the foreland basin systems in the Gangdese-Himalayan collisional orogen belt [Chinese with English abstract], *Chin. J. Geol.*, *44*(4), 1289–1311.

Ding, L., Q. Xu, Y. H. Yue, H. Wang, F. Cai, and S. Li (2014), The Andean-type Gangdese Mountains: Paleoelevation record from the Paleocene–Eocene Linzhou Basin, *Earth Planet. Sci. Lett.*, *392*, 250–264.

England, P., and M. Searle (1986), The Cretaceous-Tertiary deformation of the Lhasa block and its implications for crustal thickening in Tibet, *Tectonics*, *5*, 1–14.

Farley, K. A. (2002), (U-Th)/He dating: Techniques, calibrations, and applications, in *Noble Gases in Geochemistry and Cosmochemistry, Rev. Mineral. Geochem.*, vol. 47, edited by D. Porcelli, C. J. Ballentine, and R. Wieler, pp. 819–844, Mineral. Soc. Amer., Washington, D. C.

Farley, K. A., R. A. Wolf, and L. T. Silver (1996), The effects of long alpha-stopping distances on (U-Th)/He ages, *Geochim. Cosmochim. Acta*, *60*, 4223–4229.

Flowers, R. M., R. A. Ketcham, D. L. Shuster, and K. A. Farley (2009), Apatite (U-Th)/He thermochronometry using a radiation damage accumulation and annealing model, *Geochim. Cosmochim. Acta*, *73*, 2347–2365.

Gleadow, A., D. X. Belton, B. P. Kohn, and R. W. Brown (2002), Fission track dating of phosphate minerals and the thermochronology of apatite, *Rev. Mineral. Geochem.*, *48*, 579–630.

Gleadow, A. J. W., S. J. Gleadow, D. X. Belton, B. P. Kohn, M. S. Krochmal, and R. W. Brown (2009), Coincidence mapping––A key strategy for the automatic counting of fission tracks in natural minerals, *Geol. Soc. Spec. Publ.*, *324*(1), 25–36.

Guenthner, W. R., P. W. Reiners, R. A. Ketcham, L. Nasdala, and G. Giester (2013), Helium diffusion in natural zircon: Radiation damage, anisotropy, and the interpretation of zircon (U-Th)/He thermochronology, *Am. J. Sci.*, *313*(3), 145–198.

Haider, V. L., I. Dunkl, H. von Eynatten, L. Ding, D. Frei, and L. Zhang (2013), Cretaceous to Cenozoic evolution of the northern Lhasa Terrane and the Early Paleogene development of peneplains at Nam Co, Tibetan Plateau, *J. Asian Earth Sci.*, *70–71*, 79–98, doi:10.1016/j.jseaes.2013.03.005.

Harrison, T. M., P. Copeland, W. S. Kidd and A. Yin (1992), Raising Tibet, *Science*, *255*, 1663–1670, doi:10.1126/science.255.5052.1663.

Hasebe, N., J. Barbarand, K. Jarvis, A. Carter, and A. J. Hurford (2004), Apatite fission-track chronometry using laser ablation ICP-MS, *Chem. Geol.*, *207*(3-4), 135–145.

He, Z. H., D. Yang, C. Zheng, and T. W. Wang (2006), Isotopic dating of the Mamba granitoid in the Gangdese tectonic Belt and its constraint on the subduction time of the Neotethys [Chinese with English abstract], *Geol. Rev.*, *52*(1), 100–106.

Hellstrom, J. (2008), Iolite: Software for spatially resolved LA-(quad and MC) ICPMS analysis, in *Laser Ablation ICP-MS in the Earth Sciences, Curr. Pract. Outstanding Issues*, edited by P. Sylvester, pp. 343–348, Mineral. Assoc. of Can., Québec, Quebec.

Hetzel, R., I. Dunkl, V. Haider, M. Strobl, H. von Eynatten, L. Ding, and D. Frei (2011), Peneplain formation in southern Tibet predates the India-Asia collision and plateau uplift, *Geology*, *39*, 983–986, doi:10.1130/G32069.1.

House, M. A., B. P. Kohn, K. A. Farley, and A. Raza (2002), Evaluating thermal history models for the Otway basin, southeastern Australia, using (U-Th)/He and fission-track data from borehole apatites, *Tectonophysics*, *349*, 277–295.

Ji, W., F. Wu, S. L. Chung, J. X. Li, and C. Z. Liu (2009), Zircon U-Pb geochronology and Hf isotopic constraints on petrogenesis of the Gangdese batholith, southern Tibet, *Chem. Geol.*, *262*(3-4), 229–245.

Kapp, P., P. G. DeCelles, A. L. Leier, J. M. Fabijanic, S. He, A. Pullen, G. E. Gehrels, and L. Ding (2007), The Gangdese retroarc thrust belt revealed, *GSA Today*, *17*(7), 4–9, doi:10.1130/GSAT01707A.1.

Ketcham, R. A. (2005), Forward and inverse modeling of low-temperature thermochronometry data, *Rev. Mineral. Geochem.*, *58*, 275–314.

Ketcham, R. A., A. Carter, R. A. Donelick, J. Barbarand, and A. J. Hurford (2007), Improved measurement of fissiontrack annealing in apatite using C-axis projection, *Am. Mineral.*, *92*, 789–798.

Lang, K. A., and K. W. Huntington (2014), Antecedence of the Yarlung–Siang–Brahmaputra River, eastern Himalaya, *Earth Planet. Sci. Lett.*, *397*, 145–158.

Leier, A. L., P. Kapp, G. E. Gehrels, and P. G. DeCelles (2007), Detrital zircon geochronology of Carboniferous–Cretaceous strata in the Lhasa terrane, Southern Tibet, *Basin Res.*, *19*(3), 361–378.
Li, G. W., B. P. Kohn, M. Sandiford, Z. Q. Xu, and L. J. Wei (2015a), Constraining the age of Liuqu Conglomerate, southern Tibet: Implications for evolution of the India-Asia collision zone, *Earth Planet. Sci. Lett.*, *426*, 259–266, doi:10.1016/j.epsl.2015.06.010.
Li, G. W., Y. T. Tian, B. P. Kohn, M. Sandiford, Z. Q. Xu, and Z. H. Cai (2015b), Cenozoic low temperature cooling history of the Northern Tethyan Himalaya in Zedang, SE Tibet and its implications, *Tectonophysics*, *643*, 80–93, doi:10.1016/j.tecto.2014.12.014.
Li, Y., C. Wang, J. Dai, G. Xu, Y. Hou, and X. Li (2015c), Propagation of the deformation and growth of the Tibetan–Himalayan orogen: A review, *Earth Sci. Rev.*, *143*, 36–61, doi:10.1016/j.earscirev.2015.01.001.
Mo, X., Y. Niu, G. Dong, Z. Zhao, Z. Hou, S. Zhou, and S. Ke (2008), Contribution of syncollisional felsic magmatism to continental crust growth: A case study of the Paleogene Linzizong volcanic succession in southern Tibet, *Chem. Geol.*, *250*, 49–67.
Molnar, P., W. R. Boos, and D. S. Battisti (2010), Orographic controls on climate and paleoclimate of Asia: Thermal and mechanical roles for the Tibetan Plateau, *Annu. Rev. Earth Planet. Sci.*, *38*, 77–102.
Najman, Y., et al. (2012), The record of Himalayan erosion preserved in the sedimentary rocks of the Hatia Trough of the Bengal Basin and the Chittagong Hill Tracts, Bangladesh, *Basin Res.*, *24*(5), 499–519.
Paton, C., J. D. Woodhead, J. C. Hellstrom, J. M. Hergt, A. Greig, and R. Maas (2010), Improved laser ablation U-Pb zircon geochronology through robust downhole fractionation correction, *Geostand.Geoanal. Res.*, *31*(4), 331–343.
Quade, J., D. O. Breecker, M. Daeron, and J. Eilter (2011), The paleoaltimetry of Tibet: An isotopic perspective, *Am. J. Sci.*, *311*(2), 77–115.
Quidelleur, X., M. Grove, O. M. Lovera, T. M. Harrison, A. Yin, and F. J. Ryerson (1997), Thermal evolution and slip history of the Renbu Zedong Thrust, southeastern Tibet, *J. Geophys. Res.*, *102*, 2659–2679.
Reiners, P. W., T. L. Spell, S. Nicolescu, and K. A. Zanetti (2004), Zircon (U-Th)/He thermochronometry: He diffusion and comparisons with 40Ar/39Ar dating, *Geochim. Cosmochim. Acta*, *68*(8), 1857–1887.
Rohrmann, A., P. Kapp, B. Carrapa, P. W. Reiners, J. Guynn, L. Ding, and M. Heizler (2012), Thermochronologic evidence for plateau formation in central Tibet by 45 Ma, *Geology*, *40*, 187–190.
Rowley, D. B., and B. S. Currie (2006), Palaeo-altimetry of the late Eocene to Miocene Lunpola basin, central Tibet, *Nature*, *439*, 677–681, doi:10.1038/nature04506.
Seiler, C., A. J. W. Gleadow, J. M. Fletcher, and B. P. Kohn (2009), Thermal evolution of a sheared continental margin: Insights from the Ballenas transform in Baja California, Mexico, *Earth Planet. Sci. Lett.*, *285*(1-2), 61–74.
Spicer, R. A., N. B. W. Harris, M. Widdowson, A. B. Herman, S. Guo, P. J. Valdes, J. A. Wolfe, and S. P. Kelley (2003), Constant elevation of southern Tibet over the past 15 million years, *Nature*, *421*, 622–624, doi:10.1038/nature01356.
Sun, X., and P. Wang (2005), How old is the Asian monsoon system? Palaeobotanical records from China, *Palaeogeogr. Palaeoclimatol. Palaeoecol.*, *222*, 181–222.
Tapponnier, P., Z. Q. Xu, F. Roger, B. Meyer, N. Arnaud, G. Wittlinger, and J. S. Yang (2001), Oblique stepwise rise and growth of the Tibet Plateau, *Science*, *294*, 1671–1677.
Tian, Y., B. P. Kohn, A. J. W. Gleadow, and S. Hu (2013), Peneplain formation in southern Tibet predates the India-Asia collision and plateau uplift. *Comment, Geology*, *41*(9), 295–296.
van der Beek, P., J. van Melle, S. Guillot, A. Pêcher, P. W. Reiners, S. Nicolescu, and M. Latif (2009), Eocene Tibetan plateau remnants preserved in the northwest Himalaya, *Nat. Geosci.*, *2*, 364–368, doi:10.1038/ngeo503.
Vermeesch, P., (2009), RadialPlotter: A Java application for fission track, luminescence and other radial plots, *Radiat. Meas.*, *44*(4), 409–410.
Vermeesch, P., and Y. T., Tian (2014), Thermal history modelling: HeFTy vs. QTQt., *Earth Sci. Rev.*, *139*, 279–290.
Wang, C., X. Zhao, Z. Liu, P. C. Lippert, S. A. Graham, R. S. Coe, H. Yi, L. Zhu, S. Liu, and Y. Li (2008), Constraints on the early uplift history of the Tibetan Plateau, *Proc. Natl. Acad. Sci. U. S. A.*, *105*(13), 4987–4992.
Wang, C., J. Dai, X. Zhao, Y. Li, S. A. Graham, D. He, and J. Meng (2014), Outward-growth of the Tibetan Plateau during the Cenozoic: A review, *Tectonophysics*, *621*, 1–43, doi:10.1016/j.tecto.2014.01.036.
Wang, E., P. J. Kamp, G. Q. Xu, K. V. Hodges, K. Meng, L. Chen, G. Wang, and H. Luo (2015), Flexural bending of southern Tibet in a retro foreland setting, *Sci. Rep.*, *5*, 12076, doi:10.1038/srep12076.
Wang, J., X. M. Hu, E. Garzanti, and F. Wu (2013), Upper Oligocene–Lower Miocene Gangrinboche Conglomerate in the Xigaze Area, Southern Tibet: Implications for Himalayan Uplift and Paleo-Yarlung-Zangbo Initiation, *J. Geol.*, *121*(4), 425–444.
Woodhead, J., J. Hergt, M. Shelley, S. Eggins, and R. Kemp (2004), Zircon Hf-isotope analysis with an excimer laser, depth profiling, ablation of complex geometries, and concomitant age estimation, *Chem. Geol.*, *209*, 121–135, doi:10.1016/j.chemgeo.2004.04.026.
Woodhead, J. D., J. Hellstrom, J. M. Hergt, A. Greig, and R. Maas (2007), Isotopic and elemental imaging of geological materials by laser ablation inductively coupled plasma-mass spectrometry, *Geostand. Geoanal. Res.*, *31*(4), 331–343.
Wu, F. Y., W. Q. Ji, C. Z. Liu, and S. L. Chung (2010), Detrital zircon U-Pb and Hf isotopic data from the Xigaze fore-arc basin: Constraints on Transhimalayan magmatic evolution in southern Tibet, *Chem. Geol.*, *271*(1-2), 13–25.
Yin, A. (2006), Cenozoic tectonic evolution of the Himalayan orogen as constrained by along strike variation of structural geometry, exhumation history, and foreland sedimentation, *Earth Sci. Rev.*, *76*, 1–131.
Yuan, W. M., Y. S. Du, L. Q. Yang, S. R. Li, and J. Q. Dong (2007), Apatite fission track studies on the tectonics in Nanmulin area of Gangdese terrane, Tibetan Plateau [Chinese with English abstract], *Acta Petrol. Sin.*, *23*(11), 2911–2917.
Zhou, S., X. X. Mo, G. C. Dong, Z. D. Zhao, R. Z. Qiu, T. Y. Guo, and L. L. Wang (2004), 40Ar-39Ar geochronology of Cenozoic Linzizong volcanic rocks from Linzhou Basin, Tibet, China, and their geological implications, *Chin. Sci. Bull.*, *49*, 1970–1979
Zhu, D. C., Z. D. Zhao, Y. L. Niu, X. Mo, S. Chung, Z. Hou, L. Wang, and F. Wu (2011), The Lhasa Terrane: Record of a microcontinent and its histories of drift and growth, *Earth Planet. Sci. Lett.*, *301*, 1–22.